View metadata, citation and similar papers at core.ac.uk
brought to you by CORE
provided by Institute of Transport Research:Publications
Check for updates

applied optics

Simulation and optimization of a broadband reflective far ultraviolet polarimeter

Maëlle Le Gal,[1,*] Arturo López Ariste,[2] Coralie Neiner,[1] and Martin Pertenais[3]

[1]LESIA, Observatoire de Paris, Université PSL, CNRS, Sorbonne Université, Université de Paris, 5 place Jules Janssen, 92195 Meudon, France
[2]IRAP, Université de Toulouse, CNRS, CNES, UPS. 14, Av. E. Belin., 31400 Toulouse, France
[3]Deutsches Zentrum für Luft- und Raumfahrt e.V. (DLR), Institute of Optical Sensor Systems, Rutherfordstr. 2, 12489 Berlin, Germany
*Corresponding author: maelle.le-gal@obspm.fr

Received 3 July 2020; revised 14 September 2020; accepted 16 September 2020; posted 17 September 2020 (Doc. ID 397984); published 14 October 2020

Traditional transmissive polarimetric methods can be used for wavelengths above 123 nm where birefringent materials transmit light and create significant birefringence. Below 123 nm, no suitable solution is known to measure the four Stokes parameters on a large wavelength range. Therefore, we study here an innovative reflective (rather than transmissive) polarimeter working in the far ultraviolet (FUV) range from 90 to 130 nm. We take advantage of the phase shift created by reflections as well as the different reflectivities for p (orthogonal ⊥) and s (parallel ∥ to the plane of incidence) polarizations to design an FUV polarimeter. Simulation of the analyzer and modulator using Mueller matrices coupled to polarimetric efficiencies calculations allowed optimization of reflective polarimeters for the first time, to the best of our knowledge. This opens up a new perspective for FUV polarimetry below 123 nm. © 2020 Optical Society of America

https://doi.org/10.1364/AO.397984

1. INTRODUCTION

A. POLLUX for LUVOIR

For the 2020 NASA decadal survey, the large ultraviolet optical infrared surveyor (LUVOIR) [1], a 15 m diameter space telescope in its version A, is being studied. LUVOIR has the ambition to become a serviceable space telescope working from ultraviolet (UV) to infrared (IR). It is proposed to harbor four instruments, including POLLUX, a high-resolution spectropolarimeter working in the UV domain from 90 to 400 nm. POLLUX would enable the study of various topics such as galactic and stellar formation and reflected light from exoplanets or stellar magnetosphere [2]. To do so, POLLUX requires us to measure the full Stokes vector (I, Q, U, V) and to have a spectral resolution of 120,000 and a polarimetric precision of 10^{-4} at all wavelengths. To maximize instrument performance, the wavelength range of POLLUX is divided into three channels: the FUV from 90 to 124.5 nm, the mid-UV (MUV) from 118 to 200 nm, and the near UV (NUV) [3] from 200 to 400 nm. For the NUV channel, transmissive polychromatic polarimeters are being considered [4,5]. For the MUV and FUV, such solutions are either not ideal or simply impossible. Therefore, we study here reflective polychromatic polarimeters.

B. General Principles

All polarimeters, which are currently considered for POLLUX, use temporal modulation, as illustrated in Fig. 1. As traditional sensors (e.g., CCD, CMOS, MCP) are not sensitive to the polarization of light but only to its intensity, we need to record the information of the polarization state into intensities. Modulating the polarization means to encode polarization information into the measured intensities. Temporal modulation means successive intensity measurements by the detector with different amounts of polarization encoded. The successive measurements are then combined to obtain the polarization of the source. In order to achieve that modulation, the polarimeter is made of two parts: the modulator, which takes several angular positions around the optical axis and rotates the polarization between the different Stokes parameters; and the analyzer, which filters the light polarized along one linear direction. To measure all four Stokes parameters, we need at least four measurements, which means four angular positions of the modulator. However, we decided to consider not only the four required angular positions of the modulator but a few more for redundancy reasons in case we have an outlier. This also allows us to improve the final polarimetric extraction efficiency. [6]

Commonly, polarimeters use birefringent materials such as calcite or magnesium fluoride. A waveplate of birefringent material acts as the modulator, and a linear polarizer or a prism works as the analyzer. Even though magnesium fluoride can be used for

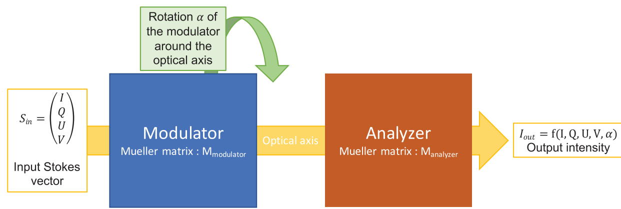

Fig. 1. General principle of a polarimeter using temporal modulation.

a waveplate almost near its transmission cutoff around 115 nm [7], its small and variable birefringence at these wavelengths makes it challenging to be used for a polychromatic polarimeter. Therefore, below ∼123 nm [4], one needs to find another way. To measure polarization as low as 90 nm, one must resort to reflection rather than the usual transmissive methods. Each reflection introduces a phase shift between p and s polarizations as well as a change in the total rate of polarization thanks to the different reflectivities. This makes it possible to use reflection for the modulator and analyzer functions. Here, we study a polarimeter made of four reflecting surfaces. Three surfaces are at a fixed position with respect to each other but free to rotate together around the optical axis; thus, they make the modulator. We choose to have three surfaces, as it is the minimum number that permits not to change the optical axis while maximizing the flux. The analyzer is made of a single reflecting surface (a dielectric crystal or a metal at a Brewster angle, which we define as the incidence angle at which the reflected beam is optimally polarized, though seldom polarized at 100% contrary to dielectrics), which polarizes the incoming light. Contrary to transmissive polarimeters, which can use dual-beam polarizers [8, 9], the use of the Brewster angle in this reflective polarimeter implies a single beam output. A scheme of this polarimeter is shown in Fig. 2. The alignment of such a device is tricky: the rotation of the modulator is likely to wobble the beam if not aligned exactly. In order to qualify for a space mission, the alignment should resist the vibration of a launch or be corrected in space. Thus, the accuracy and stability of the alignment are a major issue that will be studied later for the case of POLLUX.

C. Matrix Calculations/Mueller Calculus

In what follows, we study polarimetry using Stokes parameters and Mueller calculus. The simulation of polarimeters and the data processing involve Mueller matrices. We recall that a Mueller matrix is a 4 × 4 matrix that characterizes how a component, C, affects the polarization: the input Stokes vector S_{in} and the output Stokes vector S_{out} are linked by

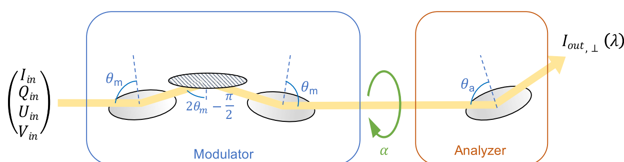

Fig. 2. Scheme of the reflective polarimeter.

$$\mathbf{S_{out}}=\begin{pmatrix}I'\\Q'\\U'\\V'\end{pmatrix}=\mathbf{M_C}*\mathbf{S_{in}}=\mathbf{M_C}*\begin{pmatrix}I\\Q\\U\\V\end{pmatrix}, \tag{1}$$

where $\mathbf{M_C}$ is the Mueller matrix of the optical component C. The four lines and four columns of the matrix correspond to the Stokes parameters I, Q, U, and V and show how the component changes the polarization among the four parameters. Each optical element has its own characteristic Mueller matrix. In particular, both the modulator and the analyzer are represented by such matrices. The Mueller matrix of the modulator can be computed with the Mueller matrix of each reflection as well as by using the rotation matrix, a 4 × 4 matrix that encodes the rotation of a component with respect to the optical axis. Mueller matrices form a group under matrix multiplication; therefore, the global Mueller matrix of the polarimeter can easily be obtained from Eq. (1) as

$$\mathbf{S_{out}}=\left(\prod_{i\in[C]}\mathbf{M_i}\right)_{\alpha}*\mathbf{S_{in}}=\mathbf{M_{polarimeter_{\alpha}}}*\mathbf{S_{in}}, \tag{2}$$

thus

$$\mathbf{M_{polarimeter_{\alpha}}}=\prod_{i\in[C]}\mathbf{M_{i\alpha}}, \tag{3}$$

where $\mathbf{M_{i_\alpha}}$ is the Mueller matrix for a component in the ensemble of components $[C]$ in the system, and $\mathbf{M_{polarimeter_{\alpha}}}$ is the Mueller matrix of the whole polarimeter for the position of the modulation α. Since we measure only intensities, we are only interested in the first component of $\mathbf{S_{out}}$, which gives the total intensity measured on the detector. We define the modulation matrix $\mathbf{O}$, which is a matrix of dimensions 4 × N formed by combining every first line of the polarimeter Mueller matrix for each of the N modulation angles (we shall often have $N=6$ in the rest of this work).

This modulation matrix $\mathbf{O}$ allows us to write an equation for the measurement process:

$$\mathbf{I_{out}}=\begin{pmatrix}I'_{\alpha_1}\\I'_{\alpha_2}\\\vdots\\I'_{\alpha_N}\end{pmatrix}=\mathbf{O}*\mathbf{S_{in}}, \tag{4}$$

with $\mathbf{I_{out}}$ the vector of the series of N intensity measurements made for each angle α of modulation and $\mathbf{S_{in}}$ the Stokes vector we want to measure. To retrieve the Stokes vector, we need the demodulation matrix $\mathbf{D}$, which is the pseudo-inverse of the modulation matrix $\mathbf{O}$ [10]:

$$\mathbf{D}=(\mathbf{O}^T*\mathbf{O})^{-1}*\mathbf{O}^T. \tag{5}$$

We then have

$$\mathbf{S_{in}}=\mathbf{D}*\mathbf{I_{out}} \tag{6}$$

to retrieve directly the initial Stokes vector from the N intensity measurements. The demodulation matrix also allows us to determine the efficiency of the polarimeter (see Section 4).

After fully studying the reflection in Section 2, we first simulate and optimize the analyzer independently using the contrast and figures of merit in Section 3. Using the results obtained for the analyzer, we finalize the polarimeter by optimizing the modulator according to the global polarimetric efficiency in Section 4.

2. SIMULATING A REFLECTION AS A MUELLER MATRIX

A. Mueller Matrix of a Reflection

To simulate and optimize a reflective polarimeter, we need to calculate its modulation and demodulation matrices from the Mueller matrices of the components, i.e., with Mueller matrices of a reflection. The Mueller matrix of a reflection $\mathbf{M_R}$ at an incidence angle θ and for a wavelength λ is given by [11]

$$\mathbf{M_R}(\theta,\lambda)=\begin{pmatrix} X(\theta,\lambda)^2+1 & X(\theta,\lambda)^2-1 & 0 & 0 \\ X(\theta,\lambda)^2-1 & X(\theta,\lambda)^2+1 & 0 & 0 \\ 0 & 0 & 2X(\theta,\lambda)\cos(\tau(\theta,\lambda)) & 2X(\theta,\lambda)\sin(\tau(\theta,\lambda)) \\ 0 & 0 & -2X(\theta,\lambda)\sin(\tau(\theta,\lambda)) & 2X(\theta,\lambda)\cos(\tau(\theta,\lambda)) \end{pmatrix} \tag{7}$$

with $X^2=r_\parallel^2/r_\perp^2$ the squared ratio of Fresnel amplitude reflection coefficients and τ the difference of phase shift between p and s polarizations. To study the modulation and efficiency of the reflective polarimeter, these two parameters must be known. This matrix is obviously dependent on the angle of incidence θ and the wavelength λ but also on the material used (optical indices of the substrate, of the coating, and of its thickness).

We present below three cases, depending on the surface used to reflect (absorbing or not) and with or without a coating. We did not consider the case of multilayer coatings.

B. Phase Shift and Amplitude of a Reflection on an Absorbing Surface with a Nonabsorbing Coating

A reflection on an absorbing material creates a phase shift in addition to the polarization-dependent reflectivities. As shown in Fig. 3, we call 1 the environment of the instrument, vacuum in our case; 2 the coating; and 3 the substrate of the surface. The indices of all the parameters in this section will refer to this notation. One may notice that the calculation of the refraction angle using Snell–Descartes equations should use the complex optical index to take the absorption into account and may provide mathematical complex refraction angles [12].

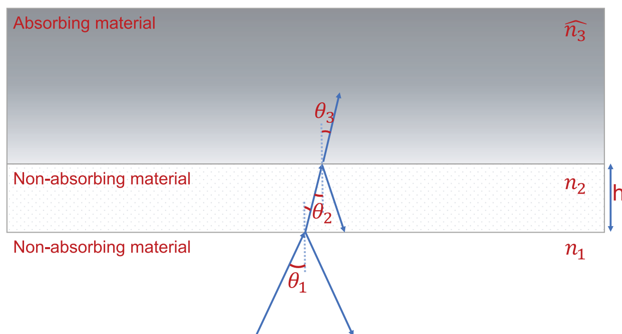

Fig. 3. Reflection on a coated absorbing surface.

The rate of reflectivities χ and the phase difference τ in this case can be directly found in [13]. Explicitly, they are calculated using the reflection coefficient r:

$$r=\frac{r_{12}+\rho_{23}e^{i(\phi_{23}+2\beta)}}{1+r_{12}\rho_{23}e^{i(\phi_{23}+2\beta)}}, \tag{8}$$

with $\beta=2\pi n_2\frac{h}{\lambda}\cos(\theta_2)$, where r_{12} is the reflection ratio at the interface between 1 and 2, and ρ_{23} and ϕ_{23} are the amplitude ratio and phase change at the interface between 2 and 3. The amplitude and phase of this reflection coefficient give the reflectivities and phases for p or s polarizations, using the appropriate expressions.

Using Born and Wolf equations [13], it is now possible to calculate χ and τ and retrieve the Mueller matrix of a reflection in the case of a coated reflecting surface.

C. Phase Shift and Amplitude of a Reflection on an Absorbing Surface Without Coating

Although a particular case of a coated surface, it is worth to recall here also the case of an uncoated substrate, which, obviously, can be computed with simpler expressions. These can also be found in [11]:

$$\chi^2=\frac{f^2+g^2-2f*\sin(\theta_1)*\tan(\theta_1)+\sin^2(\theta_1)*\tan^2(\theta_1)}{f^2+g^2+2f*\sin(\theta_1)*\tan(\theta_1)+\sin^2(\theta_1)*\tan^2(\theta_1)} \tag{9}$$

and

$$\tan(\tau)=\frac{2g*\sin(\theta_1)*\tan(\theta_1)}{\sin^2(\theta_1)*\tan^2(\theta_1)-(f^2+g^2)} \tag{10}$$

with θ_1 the angle of incidence, and where

$$f^2=\frac{1}{2}(n^2-k^2-\sin^2(\theta_1)+\sqrt{(n^2-k^2-\sin^2(\theta_1))^2+4n^2k^2} \tag{11}$$

and

$$g^2=\frac{1}{2}(k^2-n^2+\sin^2(\theta_1)+\sqrt{(n^2-k^2-\sin^2(\theta_1))^2+4n^2k^2} \tag{12}$$

help to simplify the expressions, and k is defined by $\hat{n}=n+ik$. Other terms use the same notations as in Section B.

D. Phase Shift and Amplitude of a Reflection on Nonabsorbing Material ($k=0$)

In the particular case of a nonabsorbing medium, such as crystal, where k is considered null, the expressions for reflectivities reduce to the well-known expressions. We stress that, in this case, there is no phase shift between the polarizations. Indeed, at each reflection of light coming from vacuum into the crystal, the phase shift is 0, unless the crystal is finite with width d and transparent enough so that multiple reflections occur [14]. Total reflections impose another different phase shift, used in Fresnel rhombs, but this is beyond application in our present study. Therefore, nonabsorbing media cannot be used for the modulator but can make a good polarizer.

For any given wavelength, it is indeed possible to find an angle for which the reflected beam is 100% polarized: the Brewster angle $\theta_B = \arctan(n)$. Such a Brewster angle is wavelength-dependent, which complicates its use in a broadband polarimeter if the available materials have chromatic optical indices. In addition, even if the reflection at the Brewster angle is 100% polarized, the actual reflectivity may be too small, jeopardizing the throughput of any polarimeter based upon it. This will be studied further in Section 3.

3. SIMULATING THE ANALYZER

A. Polarization Contrast and Figure of Merit

Usually, above 123 nm, beam splitters are used as transmissive analyzers, as they separate the incoming beam into two linear polarization states. This has the advantage to use all the incoming flux and to have a perfect polarizer, with two 100% polarized beams. Using a reflection is more complicated. First, this FUV analyzer only reflects one linear polarization, so we lose some flux, which is precious in the UV domain. Also, the efficiency of the polarimeter decreases, as the output beam is not 100% polarized.

Our goal is to simulate and then optimize the analyzer in order to restrict these two drawbacks, i.e., to maximize the degree of polarization, the ratio of one linear polarization with respect to its orthogonal polarization, and the transmission, i.e., to retain a sufficient signal-to-noise ratio.

Two parameters are going to help us quantify their efficiency. First, we can define a contrast as the ratio between p and s polarizations:

$$C = \left| \frac{R_s - R_p}{R_s + R_p} \right|. \quad (13)$$

The contrast can help us to determine the degree of polarization of the reflection, which is linked to the efficiency of the polarimeter. This is, however, not sufficient to characterize a good analyzer, since the reflection can be fully polarized but with an extremely low reflectivity. Thus, reflectivity should be part of our characterization. To combine both parameters, reflectivity and contrast, we introduce a figure of merit (as found in a presentation of *S*. Fineschi at the workshop *Polarimetric Techniques & Technology* in March 2014):

$$\epsilon = C * \sqrt{\max(R_s, R_p)} = \left| \frac{R_s - R_p}{R_s + R_p} \right| * \sqrt{\max(R_s, R_p)}. \quad (14)$$

The figure of merit helps us to quantify and compare analyzers according to their efficiencies and reflectivities. The square root is used on the reflectivity to minimize its variation and give a larger weight to contrast.

Now that we have a way to quantify the quality of a polarizer, we can study different solutions and compare them. The study is divided in two parts: first, the solutions, including only one material (no coating) with only one parameter to study, i.e., the incidence angle; second, the study of a coated substrate, for which there is then two parameters, i.e., the incidence angle and the thickness of the coating.

B. Uncoated Surface

For a reflection made with a material without coating, we have just one parameter: the angle of incidence. For a given material and a given wavelength, a particular angle of incidence, which optimizes polarization contrast or transmission or, ideally, both, can be computed. However, the values of the optimal angle of incidence are chromatic; at best, for a given material, we can find a compromise at the price of some trade-offs. The previously defined figure of merit in Eq. (14) will help us to define that optimal solution, but it will also be used to compare different materials. The contrast alone has also been studied to underline the benefit of the defined figure of merit.

For the spectral range of POLLUX in the FUV and MUV, we have studied the following materials: calcium fluoride (CaF_2), magnesium fluoride (MgF_2), silicon dioxide (SiO_2), gold (Au), boron carbid (B_4C), tetrahedral amorphous carbon (ta-C, a diamond-like carbon), and silicon carbide (SiC). We identified those materials in the literature, as they seem to have good reflectivity in the considered wavelength range [15–17]. The contrast as a function of incidence angle and wavelength is shown in Fig. 4. The figure of merit as a function of incidence angle and wavelength is given in Fig. 5.

Figure 4 shows that the contrast is sufficiently high for some materials such as CaF_2, MgF_2, SiO_2, Au, and ta-C to consider them. Moreover, the variation of the contrast with wavelength is acceptable in the considered wavelength range. However, in Fig. 5, one can see that, in spite of the good contrast, the reflectivity is not very high and is mostly responsible for the degradation of the efficiency of these polarizers.

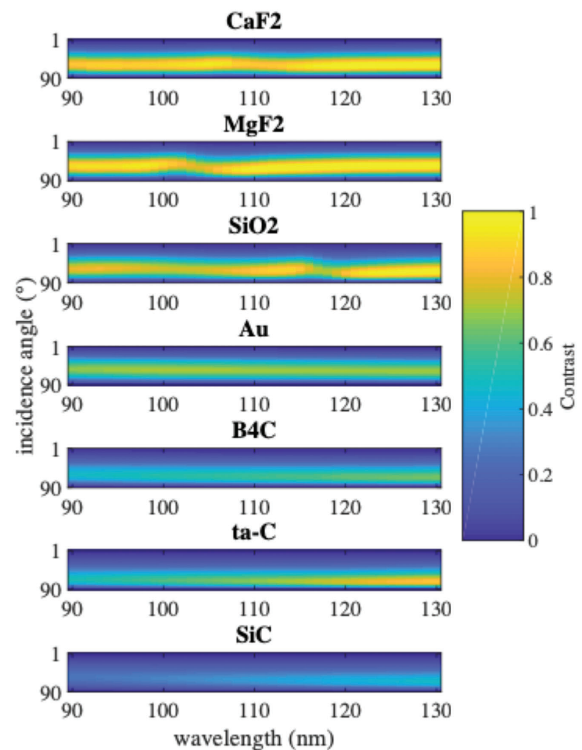

Fig. 4. Contrast after reflection on various materials as a function of wavelength and angle of incidence. At a contrast of 1, the beam after reflection is fully polarized. At a contrast of 0, the beam is not polarized.

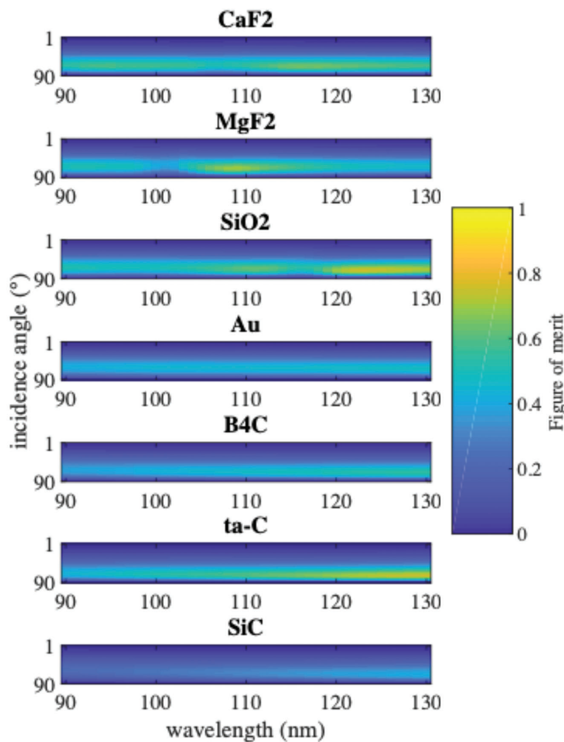

Fig. 5. Figure of merit after reflection on various materials as a function of wavelength and angle of incidence. At a figure of merit of 1, the beam after reflection is fully polarized and with no loss of flux. At a contrast of 0, the beam is not polarized and/or the flux is lost.

To compare our solutions, the mean contrast (Fig. 6) and figure of merit (Fig. 7) averaged over the considered wavelength range are plotted as a function of incidence angle. On those graphs, one can see clearly that, even though ta-C isn't the best analyzer based on contrast, reaching almost 0.7, it is the best choice when based on the figure of merit, where it hits 0.6. CaF_2 and SiO_2 seem to be good backup solutions since they have good figures of merit almost reaching 0.6. One may notice that they also have good contrast, around 0.9 for CaF_2 and 0.8 for SiO_2. The figure of merit helps us to choose ta-C reflection as

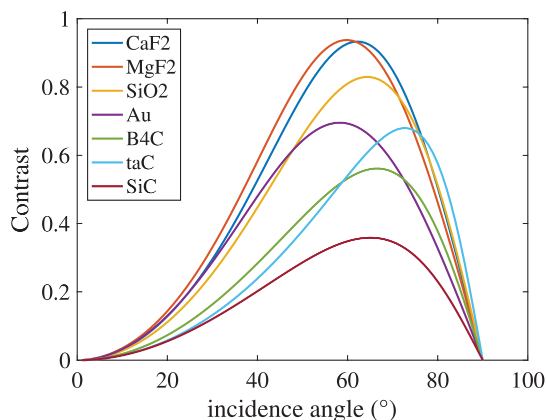

Fig. 6. Contrast of a polarizer (averaged across the spectrum) made with a reflection on various materials as a function of angle of incidence. At 1, the beam after reflection is fully polarized. At 0, the beam is not polarized.

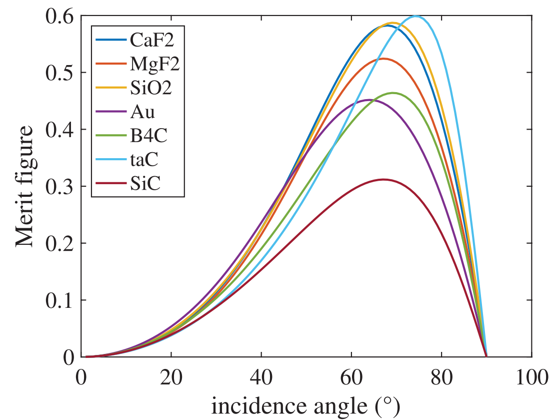

Fig. 7. Figure of merit of a polarizer (averaged across the spectrum) made with a reflection on various materials as a function of angle of incidence. At 1, the beam after reflection is fully polarized. At 0, the beam is not polarized.

the analyzer for POLLUX, as it is the best compromise between reflectivity and contrast, but this decision could be modified for a CaF_2 or a SiO_2 plate to improve the contrast and thus the efficiency of the polarimeter if the global signal-to-noise ratio obtained with POLLUX permits it. These figures show that, at maximum contrast, a tolerance of 1 deg in the incidence angle creates a loss of contrast of less than 1%.

Considering the reflectivity, we conclude that the best polarizer for the 90–130 nm wavelength domain is a plate of ta-C at 74.3° with a mean of 0.599 for the figure of merit and 0.6762 for the contrast. Nevertheless, if there were spectral lines at specific wavelengths of particular scientific interest, the choice of the polarizer could be reconsidered by adding weights to those particular wavelengths. In addition, to study particularly bright objects, a plate of CaF_2 or SiO_2 could be a better choice, as those materials improve overall efficiency, even though they decrease reflectivity.

C. Study on Coated Materials

To simulate the use of a coated material, the thickness of the coating is another parameter to consider. Thicknesses between 5 and 90 nm are considered and cover the usual values. We decided to study a reflection on aluminum coated with MgF_2 [18], as it is a well-known combination to study UV light. To analyze the two relevant parameters (incidence angle and thickness), we plot the contrast averaged over wavelength as a function of incidence angle in Fig. 8 for several thicknesses. Thicknesses were studied from 5 to 90 nm with a 1 nm step, but fewer values are displayed for clarity. A maximum contrast of 0.12 is obtained for a thickness of 32 nm, which is much lower than contrasts found for noncoated materials, which are up to 0.9. This case is therefore discarded for the analyzer of POLLUX.

Other combinations of materials for the substrate and coatings may be considered in the future, if an efficient combination appears from the current LUVOIR R&D studies.

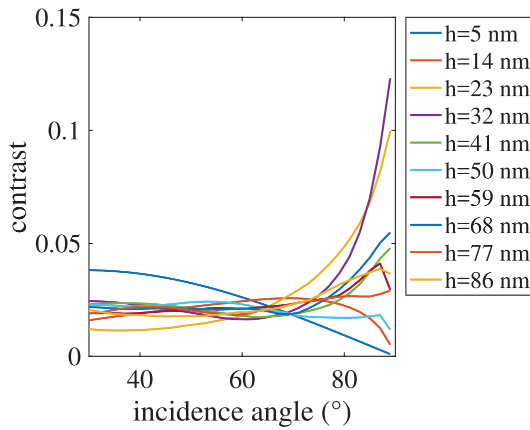

Fig. 8. Mean of contrast on wavelength of a reflective polarizer made with an aluminium mirror coated with different thicknesses (h) of MgF_2 as a function of angle of incidence. At 1, the beam after reflection is fully polarized. At 0, the beam is not polarized.

4. POLARIMETER MODULATION

A. Mueller Matrix of the Modulator

As mentioned in Subsection 1B, the modulator is formed by three reflections, so that the beam is not deviated from the optical axis, and the output beam does not move with the rotation of the modulator. The first and third reflections are then symmetrical with respect to the second one, which has its normal perpendicular to the optical axis of the instrument. The three reflections are studied as a whole and not independently, since it is the total change of phase that is of interest. To that effect, the Mueller matrix of the modulator must be computed. The studied parameter is the incidence angle θ_m on the first surface, as denoted in Fig. 2. The incidence on the other surfaces can be computed from θ_m.

The Mueller matrix of the modulator is easily built up as the product of the matrices of these three reflections. Following the notation from Fig. 2, we have $\mathbf{M_3} = \mathbf{M_R}(\theta_m, \lambda) * \mathbf{M_R}(2\theta_m - \frac{\pi}{2}, \lambda) * \mathbf{M_R}(\theta_m, \lambda)$.

The three reflecting surfaces are allowed to rotate around the optical axis, and the combined Mueller matrix is then modified by the rotation matrix of the angle of this rotation α:

$$\mathbf{R}(\alpha) = \begin{pmatrix} 1 & 0 & 0 & 0 \\ 0 & \cos(2\alpha) & \sin(2\alpha) & 0 \\ 0 & -\sin(2\alpha) & \cos(2\alpha) & 0 \\ 0 & 0 & 0 & 1 \end{pmatrix}. \quad (15)$$

The measurement of polarization with our present design consists in choosing a set of N angular positions for the modulator that differently encode polarization into intensity variations. Each one of the N measurements is differentiated by α, the rotation angle; further, the resulting Mueller matrix for the full modulator is

$$\begin{aligned}\mathbf{M_{modulator}} &= \mathbf{R}(-\alpha) * \mathbf{M_3} * \mathbf{R}(\alpha) \\ &= \mathbf{R}(-\alpha) * \mathbf{M_R}(\theta_m, \lambda) * \mathbf{M_R}\left(2\theta_m - \frac{\pi}{2}, \lambda\right) \\ &\quad * \mathbf{M_R}(\theta_m, \lambda) * \mathbf{R}(\alpha). \end{aligned} \quad (16)$$

However, as seen in previous sections, we cannot find a perfect analyzer. The solutions found for POLLUX polarizes light but not completely; in the case of ta-C, we even expect a retardance phase to appear between the reflected orthogonal polarizations. In other words, the analyzer may not just be polarizing but also transforming, rotating one polarization into another, a role that, in theory, we reserved to the modulator. Because of this, we cannot study or optimize the modulator alone. We must consider the whole polarimeter made of the rotating three-reflections modulator plus the nonperfect analyzer.

B. Optimizing the Polarimeter

To study and optimize the modulator, we must also study the analyzer, i.e., the Mueller matrix of the complete polarimeter must be studied. We can easily compute the Mueller matrix for the whole polarimeter from the modulator Mueller matrix computed in Section B. The Mueller matrix for the whole polarimeter is

$$\begin{aligned}\mathbf{M_{polarimeter}} &= \mathbf{M_{analyzer}}(\theta_a) * \mathbf{R}(-\alpha) * \mathbf{M_3} * \mathbf{R}(\alpha) \\ &= \mathbf{M_{analyzer}}(\theta_a) * \mathbf{R}(-\alpha) * \mathbf{M_R}(\theta_m, \lambda) \\ &\quad * \mathbf{M_R}\left(2\theta_m - \frac{\pi}{2}, \lambda\right) * \mathbf{M_R}(\theta_m, \lambda) * \mathbf{R}(\alpha). \end{aligned} \quad (17)$$

Choosing a set of modulation angles α and keeping only the intensity of the resulting Stokes vector for each one of those angles, we can build the modulation matrix $\mathbf{O}$, as described in Section C, which relates the incoming Stokes vector to the actual series of intensity measurements. An example of this modulation matrix is shown in Fig. 9.

To quantify the performances of the whole polarimeter and optimize it, we define, following [10], a polarimetric efficiency as

$$\epsilon_i = \left(N \sum_{j=1}^{N} \mathbf{D}_{ij}^2 \right)^{-1/2} \quad (18)$$

of a given demodulation scheme made of N measurements and represented by matrix $\mathbf{D}$, the pseudo-inverse of the modulation matrix $\mathbf{O}$, for every Stokes parameter $i \in [I, Q, U, V]$. It is important to stress that the three efficiencies for Q, U, and V obey the relationship

$$\sum_{Q,U,V} \epsilon_i^2 \leq 1. \quad (19)$$

Our work in optimizing the modulator has been to pick the material, incidence angle θ_m, and set of modulation angles α, which maximize these efficiencies ϵ_i. The need for good reflectivity limits the materials available for the modulator to the same ones as those studied for the analayzer, i.e., SiC, ta-C, Al + MgF2... Crystals cannot be used for modulation because they do not introduce any phase shift between polarizations.

The incidence angle θ_m and modulation angles α have been fixed through a Marquardt–Levenberg iteration scheme with the constraint to minimize the difference between their value

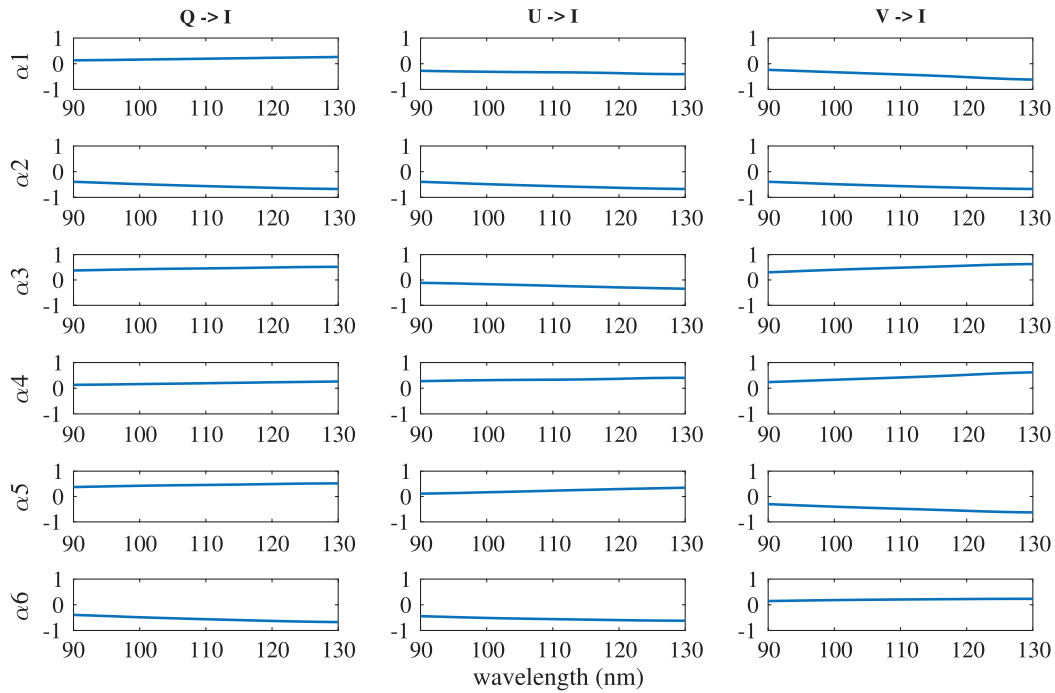

Fig. 9. Modulation matrix of a polarimeter made with one surface of B_4C and two surfaces of SiC and a ta-C analyzer.

and the maximum theoretical one. The maximum theoretical efficiency is $1/\sqrt{3}$ in our case, since we choose to measure the three Stokes parameters with identical efficiency. This can be changed to highlight a particular Stokes parameter to satisfy scientific specification. The incidence angle and modulation angles have been optimized for all combinations of materials for the three reflections, including mixing and matching different materials in order to find the best polarimeter.

The actual number of measurements N, however, has been fixed by simple comparison of the best solutions obtained in each situation. A minimum of $N = 4$ is required to retrieve the four Stokes parameters, but increasing the number of measurements will improve the signal-to-noise ratio attributed to each Stokes vector. This may improve overall efficiency. To compromise between redundancy and convenience, we chose $N = 6$ for our polarimeter.

This optimization on the materials, incidence angle, and modulation angles has converged to one efficient modulator working from 90 to 130 nm. The first reflection is in B_4C and the two others are in SiC. The incidence angle is $\theta_m = 86.8°$. The modulator takes six angular positions: 15.8°, 48.4°, 66.0°, 114.0°, 131.6°, and 164.2°. Figure 10 shows the efficiencies in the three Stokes parameters Q, U,

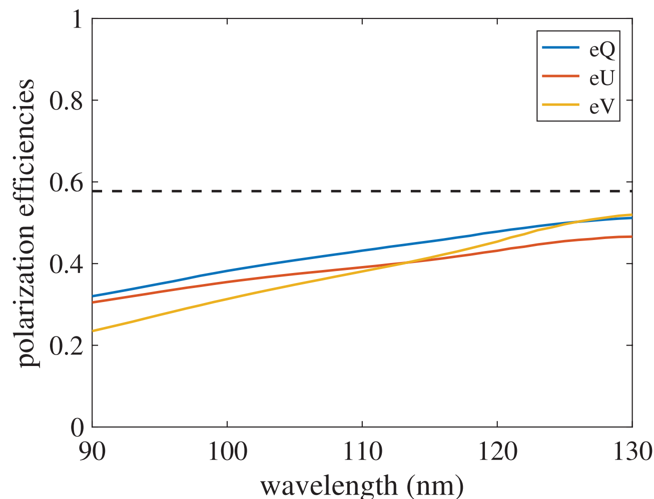

Fig. 10. Polarimetric efficiencies of a polarimeter by reflection with a B_4C and SiC modulator and a ta-C analyzer. The black dotted line is the optimal efficiency at 57.7% we try to achieve.

and V as a function of wavelength for this modulator and a ta-C analyzer. The black dotted line is the optimal efficiency to measure the three Stokes parameters with the same efficiency. The efficiencies are around 0.3 at 90 nm and increase with wavelength to obtain a satisfying result around 0.55 at 130 nm. The sensibility of the modulator is thinner than the one of the polarizer. Indeed, a change of 0.1 degree in the incidence angle on the first mirror implies a change up to 0.04 in the polarization efficiencies.

5. CONCLUSION

We have studied and optimized, for the first time to our knowledge, a new polarimeter design using only reflection on different surfaces and working in the FUV on a large spectrum. The modulator is made with three surfaces, fixed with respect to one another, and rotating as a block to create a temporal modulation of the polarization. The analyzer is the critical part of the design, as one has to make a trade-off between efficiency and reflectivity. A plate at the Brewster angle or a reflecting surface at a similar angle can play the role of the analyzer. This design has the benefit of not deviating the optical axis with the rotation of the modulator. The optimal polarimeter for the wavelength range 90–130 nm calculated for POLLUX is made of one reflection in B_4C and two reflections in SiC for the modulator. The analyzer has several options, the one maximizing the flux is a reflection in ta-C. A plate of CaF_2 or SiO_2, increasing the efficiency but decreasing the reflectivity of the polarimeter, can be used for bright sources. In the case of POLLUX, we need to maximize the flux; thus, the choice of a ta-C reflection has been made, decreasing a bit the efficiency but increasing a lot the reflectivity. To confirm those theoretical results, an experiment has been set up to measure complex optical indexes for the considered materials. This experiment should be conducted in the coming year and will be the subject of a subsequent paper.

6. DATA

For calculations, the optical indexes used to compute CaF_2, MgF_2, SiO_2, Au, B_4C, and SiC are from Palik and to compute ta-C are from Juan Larruquert.

Funding. Centre National d'Etudes Spatiales.

Acknowledgment. The authors would like to thank Juan Larruquert (CSIC, Spain) for sharing his data on optical indexes, allowing these first calculations.

Disclosures. The authors declare no conflicts of interest.

REFERENCES

1. M. R. Bolcar, S. Aloezos, V. T. Bly, C. Collins, J. Crooke, C. D. Dressing, L. Fantano, L. D. Feinberg, K. France, G. Gochar, Q. Gong, J. E. Hylan, A. Jones, I. Linares, M. Postman, L. Pueyo, A. Roberge, L. Sacks, S. Tompkins, and G. West, "The large UV/optical/infrared surveyor (LUVOIR): decadal mission concept design update," Proc. SPIE **10398**, 79–102 (2017).
2. J.-C. Bouret, C. Neiner, A. I. G. de Castro, C. Evans, B. Gaensicke, S. Shore, L. Fossati, C. Gry, S. Charlot, F. Marin, P. Noterdaeme, and J.-Y. Chaufray, "The science case for POLLUX: a high-resolution UV spectropolarimeter onboard LUVOIR," Proc. SPIE **10699**, 106993B (2018).
3. M. Le Gal, M. Pertenais, A. L. Ariste, C. Neiner, N. Champion, Y. Younes, and J.-M. Reess, "VUV test of a new polarimeter for spectropolarimetric measurements on board space missions," Proc. SPIE **10706**, 107061M (2018).
4. M. Pertenais, C. Neiner, and P. Petit, "Full-Stokes polychromatic polarimeter design for Arago," Proc. SPIE **9905**, 99052Y (2016).
5. S. Tomczyk, R. Casini, A. G. de Wijn, and P. G. Nelson, "Wavelength-diverse polarization modulators for Stokes polarimetry," Appl. Opt. **49**, 3580–3586 (2010).
6. D. S. Sabatke, M. R. Descour, E. L. Dereniak, W. C. Sweatt, S. A. Kemme, and G. S. Phipps, "Optimization of retardance for a complete Stokes polarimeter," Opt. Lett. **25**, 802–804 (2000).
7. R. Ishikawa, R. Kano, T. Bando, Y. Suematsu, S.-N. Ishikawa, M. Kubo, N. Narukage, H. Hara, S. Tsuneta, H. Watanabe, K. Ichimoto, K. Aoki, and K. Miyagawa, "Birefringence of magnesium fluoride in the vacuum ultraviolet and application to a half-waveplate," Appl. Opt. **52**, 8205–8211 (2013).
8. H. Watanabe, N. Narukage, M. Kubo, R. Ishikawa, T. Bando, R. Kano, S. Tsuneta, K. Kobayashi, K. Ichimoto, and J. Trujillo-Bueno, "Ly-alpha polarimeter design for CLASP rocket experiment," Proc. SPIE **8148**, 81480T (2011).
9. R. Ishikawa, N. Narukage, M. Kubo, S. Ishikawa, R. Kano, and S. Tsuneta, "Strategy for realizing high-precision VUV spectro-polarimeter," Sol. Phys. **289**, 4727–4747 (2014).
10. J. C. del Toro Iniesta and M. Collados, "Optimum modulation and demodulation matrices for solar polarimetry," Appl. Opt. **39**, 1637–1642 (2000).
11. C. Capitani, F. Cavallini, G. Ceppatelli, E. L. Degl'innocenti, M. L. Degl'innocenti, M. Landolfi, and A. Righini, "Polarization properties of a 'Zeiss-type' coelostat: the case of the solar tower in Arcetri," Solar Phys. **120**, 173–191 (1989).
12. S. Kovalenko, "Descartes-Snell law of refraction with absorption," Semicond. Phys. Quantum Electron. Optoelectron. **4**, 214–218 (2001).
13. M. Born and E. Wolf, *Principles of Optics: Electromagnetic Theory of Propagation, Interference and Diffraction of Light* (Elsevier, 2013).
14. M. Salatino, P. de Bernardis, and S. Masi, "Modeling transmission and reflection Mueller matrices of dielectric half-wave plates," J. Infrared Millim. Terahertz Waves **38**, 215–228 (2017).
15. J. I. Larruquert, L. V. Rodríguez-de Marcos, J. A. Méndez, P. J. Martin, and A. Bendavid, "High reflectance ta-C coatings in the extreme ultraviolet," Opt. Express **21**, 27537–27549 (2013).
16. R. Keski-Kuha, J. Larruquert, J. Gum, and C. Fleetwood, "Optical coatings and materials for ultraviolet space applications," in *Ultraviolet-Optical Space Astronomy Beyond HST* (1999), Vol. **164**, p. 406.
17. P. Zetner, A. Pradhan, W. B. Westerveld, and J. W. McConkey, "Polarization analysis techniques in the VUV," Appl. Opt. **22**, 2210–2212 (1983).
18. G. Hass and W. R. Hunter, "Reflection polarizers for the vacuum ultraviolet using Al+MgF_2 mirrors and an MgF_2 plate," Appl. Opt. **17**, 76–82 (1978).